Journal of Power Sources 188 (2009) 347–352

Contents lists available at ScienceDirect

Journal of Power Sources

journal homepage: www.elsevier.com/locate/jpowsour

Fabrication of bimetallic Pt–M (M = Fe, Co, and Ni) nanoparticle/carbon nanotube electrocatalysts for direct methanol fuel cells

Chien-Te Hsieh [a,b,*], Jia-Yi Lin [a]

[a] Department of Chemical Engineering and Materials Science, Yuan Ze University, 135 Yuan-Tung Rd., Chung-Li, Taoyuan 320, Taiwan
[b] Yuan Ze Fuel Cell Center, Yuan Ze University, Taoyuan 320, Taiwan

ARTICLE INFO

Article history:
Received 7 November 2008
Received in revised form 9 December 2008
Accepted 10 December 2008
Available online 24 December 2008

Keywords:
Pt-based nanoparticles
Bimetallic catalysts
Carbon nanotubes
Electrochemical activity
Direct methanol fuel cells

ABSTRACT

The electrochemical activities of three bimetallic Pt–M (M = Fe, Co, and Ni) catalysts in methanol oxidation have been investigated. An efficient approach including chemical oxidation of carbon nanotubes (CNTs), two-step refluxing, and subsequent hydrogen reduction was used to thoroughly disperse bimetallic nanopartilces on the oxidized CNTs. Three catalysts with a similar Pt:M atomic ratio, Pt–Fe (75:25), Pt–Co (75:25), and Pt–Ni (72:28), were prepared for the investigation of methanol oxidation. The Pt–M nanoparticles with an average size of 5–10 nm are uniform and cover the surface of CNTs. Cyclic voltammetry showed that the three pairs of catalysts were electrochemically active in the methanol oxidation. On the basis of the experimental results, the Pt–Co/CNT catalyst has better electrochemical activity, antipoisoning ability, and long-term cycleability than the other electrocatalysts, which can be justified by the bifunctional mechanism of bimetallic catalysts. The satisfactory results shed some light on how the use of Pt–Co/CNT composite could be a promising electrocatalyst for high-performance direct methanol fuel cell applications.

1. Introduction

Fuel cells have been hailed as an important power source for the future because of their high energy conversion efficiency and low environmental pollution [1–6]. The conversion of chemical energy into electricity in direct methanol fuel cells (DMFCs) requires the development of better catalysts to improve the cell performance. It is generally recognized that pure Pt electrocatalysts are prone to poisoning by CO since the CO molecules can chemically adsorb onto the Pt surface and block the active sites [7–9]. As a result, Pt catalysts rapidly deactivate owing to the formation of Pt–CO species in the electrooxidation of methanol. To date, the development of bimetallic catalysts usually consists of a primary metal that has a high performance in catalytic activity and a secondary metal that can enhance the catalytic activity or prevent poisoning problems. It has been shown that bimetallic PtRu catalysts enable the reduction of CO poisoning [8–16]. The role of ruthenium is to dissociate water to produce adsorbed OH species, which react with CO adsorbed on the Pt surface to generate CO_2. More recently, an attempt to increase the activity by alloying Pt with a second metal such as Sn [17], Co [18–20] and other metals [21–23] has been reported. The appearance of the second metals exhibited a remarkable improvement in CO tolerance and electrochemical activity. Moreover, the presence of a second element more abundant could contribute to decreasing of costs associated with Pt [18].

To improve the electrochemical activity, a common approach has been used to uniformly deposit bimetallic catalysts onto a carbon support. Commercial anode catalysts in DMFCs are frequently PtRu nanoalloys coated on carbon black in the form of well dispersion of $Pt_{50}Ru_{50}$ particles [8]. There has been increasing interest in multiwalled carbon nanotubes (CNTs) as heterogeneous catalyst supports [8–15,24], owing to their high porosity and high electrical conductivity. However, the role of deposition of bimetallic catalysts on CNT supports in the improvement of electrochemical activity in methanol oxidation has not yet been clearly elucidated. Our pervious study has shown an efficient way to deposit electrocatalysts on the sidewalls of CNTs [9,25,10]. Proper dispersion of the catalysts on CNTs would enhance the reaction kinetics and activity for methanol oxidation, since CNTs have a unique one-dimensional structure. This work aims to demonstrate the electrochemical characterization of Pt–M/CNTs electrocatalysts, including the onset potential, electrochemical activity, and cycle stability in methanol oxidation. These results would shed some light on the replacement of novel metal catalysts by using transition metals, and on how the introduction of transition metals in bimetallic catalysts enhances the electrochemical performance of methanol oxidation.

* Corresponding author at: Department of Chemical Engineering and Materials Science, Yuan Ze University, 135 Yuan-Tung Rd., Chung-Li, Taoyuan 320, Taiwan. Tel.: +886 3 4638800x2577; fax: +886 3 4559373.
E-mail address: cthsieh@saturn.yzu.edu.tw (C.-T. Hsieh).

0378-7753/$ – see front matter © 2008 Elsevier B.V. All rights reserved.
doi:10.1016/j.jpowsour.2008.12.031

2. Experimental

2.1. Synthesis of Pt–M/CNT composites

The procedure for growing different types of Pt–M (M = Fe, Co, and Ni)/CNT composites can be described as follows. In this study, multiwalled CNTs (purity: >99%; outer diameter: 30–50 nm; length: 5–10 μm) were prepared by a catalytic chemical vapor deposition technique, using ethylene and Ni particle as the carbon precursor and catalyst, respectively. A chemical-wet oxidation in nitric acid enabled the implantation of surface oxides such as carboxylic (–COOH), carbonyl (–C=O), and hydroxyl (–C–OH) groups on both ends and defects of CNTs [26,27]. The oxidized CNT samples were well dispersed in 3N nitric acid at 90 °C for 2 h. After that, oxidized CNT samples were rinsed with distilled water several times until the pH value of the carbon slurry was higher than 5. Then the CNTs were heated at 150 °C under an Ar atmosphere for 1 h.

The two-step chemical reflux process led to the deposition of bimetallic catalysts on oxidized CNTs. The first-step refluxing was applied to deposit the primary catalyst (Pt), followed by the second reflux that was used to coat the secondary catalyst (Fe, Co, and Ni) to form binary metallic catalysts. Oxidized CNTs (1 g) were mixed with a 0.1 M $PtCl_4{\cdot}5H_2O$ (Alfa Aesar) aqueous solution at ambient temperature for 8 h. The first-step reflux was preformed at 110 °C for 8 h, using 50 mL of ethylene glycol as reduction agent. Next, Pt-coated CNT composites were separated from ethylene glycol solution by using a filtration apparatus. A thermal reduction process was carried out in tubular reactor at 500 °C under 5 vol.% H_2 atmosphere to ensure reduction of Pt particles. The second-step refluxing was also conducted at 110 °C for 8 h. The Pt-attached CNTs were placed in different ionic salts: 1 M $Fe(NO_3)_2$, $Ni(NO_3)_2$ and $Co(NO_3)_2$. The reflux process allowed the uniform coating of transition metals on the Pt surface. Finally, hydrogen reduction was carried out in tubular reactor at 350 °C under 5 vol.% H_2 atmosphere for reduction of bimetallic Pt–M catalysts.

These Pt–M/CNT samples were characterized by transmission electron microscope (TEM, Hitachi H-7500) and X-ray diffraction (XRD) with Cu Kα radiation, using an automated X-ray diffractometer (Shimazu Labx XRD-6000). The TEM study was carried out using a microscope operating at 200 kV. The CNT samples for the TEM analysis were prepared by ultrasonically dispersing the catalyst powders in ethanol. A drop of the suspension was applied onto a carbon-coated copper grid and was dried in air. The XRD scans were investigated at 2 min^{-1} for 2θ values between 20° and 100°.

2.2. Electrochemical measurements of Pt–M/CNT electrodes

The as-prepared Pt–M/CNT composites were used for fabrication of electrodes. Prior to the electrochemical tests, each CNT sample was added to a solution of poly-vinylidenefluoride (PVdF) in *N*-methylpyrrolidinone (NMP), and the mixture was then mixed at ambient temperature to form a carbon slurry. Electrodes were prepared by pressing the slurry on stainless steel foils with a doctor blade, followed by evaporating the solvent, NMP, with a blower dryer. The carbon layer, which consisted of 10 wt.% PVdF and 20 wt.% graphite powder (size: 20–30 μm) as the binder and conducting material, respectively, was adjusted to have a thickness of 150 μm. Electrochemical measurements were investigated at ambient temperature using 1 M H_2SO_4 + 0.5 M CH_3OH as the electrolyte solution, using a CHI 608 electrochemical working station. A Pt wire was used as the counter-electrode, and a saturated calomel electrode (SCE) was used as the reference. The working electrodes were constructed by coating the CNTs onto a stainless steel foil (as current collector). Cyclic voltammetric (CV) measurements of the Pt–M/CNT composite electrodes were performed in the potential range of 0–1 V vs. SCE with a sweep rate of 10 mV s^{-1}. All electrochemical measurements in this study were conducted under N_2 atmosphere at ambient temperature.

3. Results and discussion

3.1. Morphology and crystalline structure of Pt–M/CNT composites

Typical SEM images for each pair of the bimetallic nanoparticles deposited on oxidized CNTs are shown in Fig. 1(a)–(d). The metal nanoparticles are homogeneously dispersed on the surface of CNT support. In comparison, the average sizes of bimetallic Pt–M particles are found to be very close to that of Pt, indicating a good incorporation of transition metals into the Pt catalyst. An analysis of energy-dispersive spectroscopy (EDS) shows that the element compositions of the bimetallic catalysts are Pt–Fe (75:25), Pt–Co (75:25), and Pt–Ni (72:28). This result can be attributed to the fact that the surface oxidation followed by the two-step refluxing technique leads to the preparation of a well-defined atomic ratio of bimetallic electrocatalysts.

Fig. 2(a)–(c) shows the results of XRD for each pair of the bimetallic nanoparticles deposited on CNTs. It is known that pure Pt has a face-centered cubic (fcc) structure. The peaks at $2\theta \approx 40°$ and 47° can be characterized with the (1 1 1) and (2 0 0) planes, respectively [28], of the fcc structure of platinum. In addition, other diffraction peaks are characterized to different types of transition metals (i.e., Fe, Co, and Ni), confirming different pairs of Pt–M catalysts on CNTs. With the addition of different types of transition metals, the diffraction peaks of binary Pt–M catalysts lead to broaden and shift to higher 2θ values [3]. As shown in Fig. 2(b), the 2θ of the (1 1 1) peak for all Pt–M particles at around 40.2° shows a slight shift, when compared with pure Pt at 39.95°. The same trend is replicated for Pt (2 2 0) diffraction. The 2θ of the (2 2 0) peak for Pt–M particles is found to have a higher value of 68.1° than 67.8° for pure Pt catalyst, demonstrated by the observation of Fig. 2(c).

The average particle size of the bimetallic catalysts can be calculated through XRD patterns according to Scherrer's formula [29,30]:

$$d_{\mathrm{XRD}} = \frac{0.9\lambda}{\beta_{1/2}\cos\theta} \quad (1)$$

where d_{XRD} is the average particle size (nm), λ the wavelength of X-ray (0.15406 nm), θ the angle at the peak maximum, and $\beta_{1/2}$ is the width (radians) of the peak at half height. The calculated mean sizes according to the diffraction peak of Pt (1 1 1) are collected as follows: 6.26 nm (Pt), 6.74 nm (Pt–Fe), 6.74 nm (Pt–Co), and 6.78 nm (Pt–Ni). After the deposition of transition metals, the larger crystalline size can be attributed to one possible reason that the two-step chemical reduction generates core–shell (Pt–M) crystalline structures. Since the transition metals cover over Pt particle, this leads to enlarge the size of the bimetallic particles.

Bright-field TEM images for CNTs decorated with different pairs of bimetallic nanoparticles are given in Fig. 3(a)–(d). These images show that the original CNTs have an average outer diameter of 30–50 nm and a wall thickness of ~10 nm. The homogeneous distribution of small and uniform dark spots corresponds to Pt–M particles, which only form on the sidewalls of CNTs. Generally, the aggregation of alloy nanoparticles is not apparent, and these nanoparticles are highly dispersed on the CNTs. All bimetallic nanoparticles display a very narrow-size distribution, showing an average particle size of 5–10 nm. Again, this deposition of uniformly dispersed metallic and bimetallic nanoparticles on CNTs is believed to be the result of uniform surface functional sites on all nanotubes that can be created in the chemical-wet oxidation of nitric acid [25].

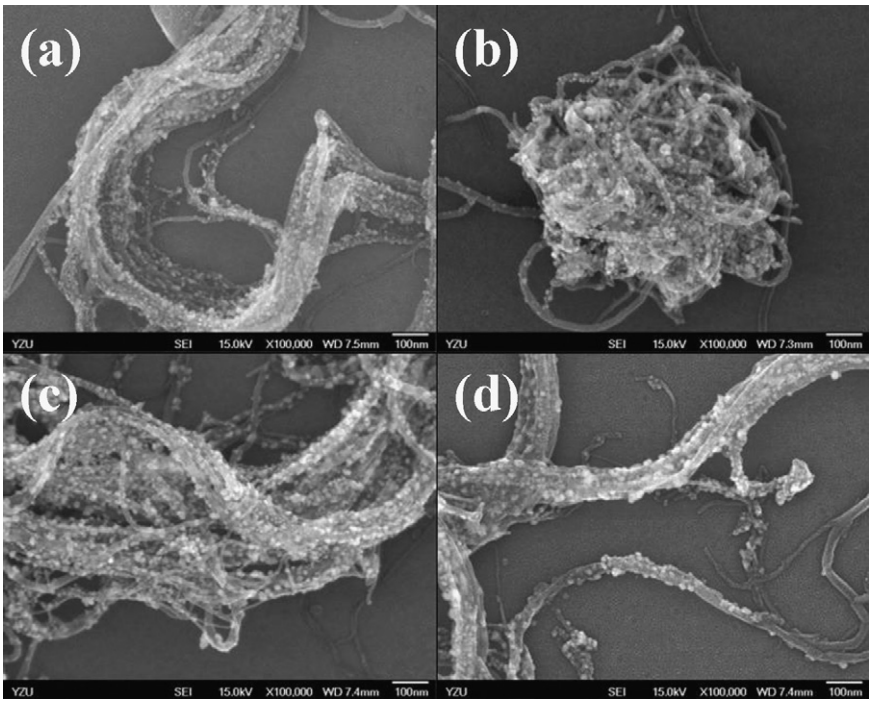

Fig. 1. SEM images of different types of Pt and Pt–M/CNT samples: (a) Pt, (b) Pt–Fe, (c) Pt–Co, and (d) Pt–Ni. The scale bar is 100 nm.

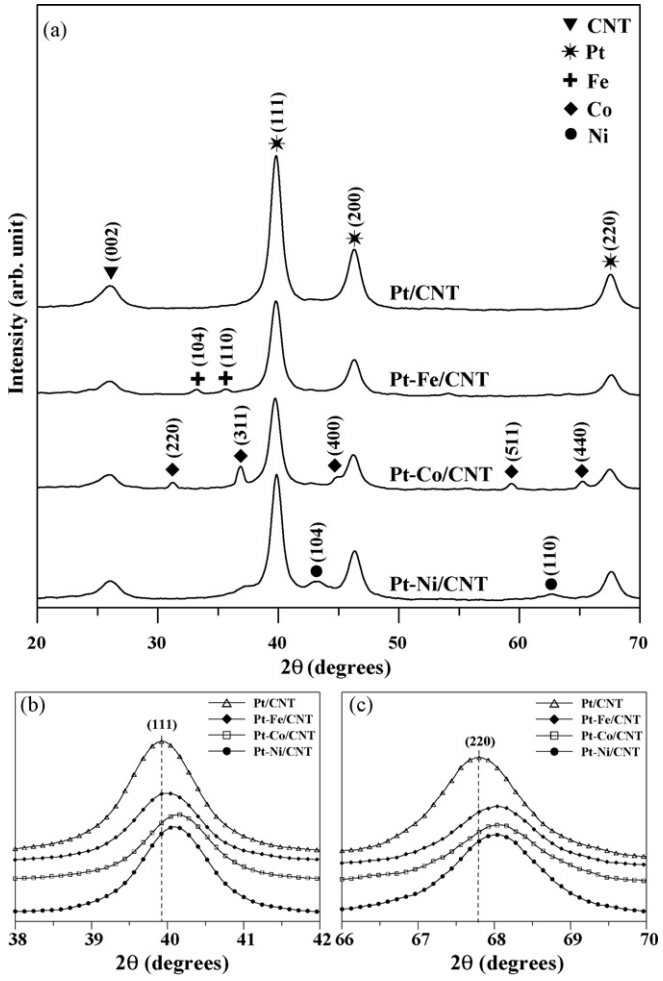

Fig. 2. (a) X-ray diffraction patterns of different types of Pt and Pt–M/CNT samples, showing characteristics crystalline faces of Pt and transition metals. The peak of C was identified as graphite from CNTs. X-ray diffraction patterns of (b) Pt (1 1 1) and (c) Pt (2 2 0) for different types of Pt and Pt–M/CNT samples.

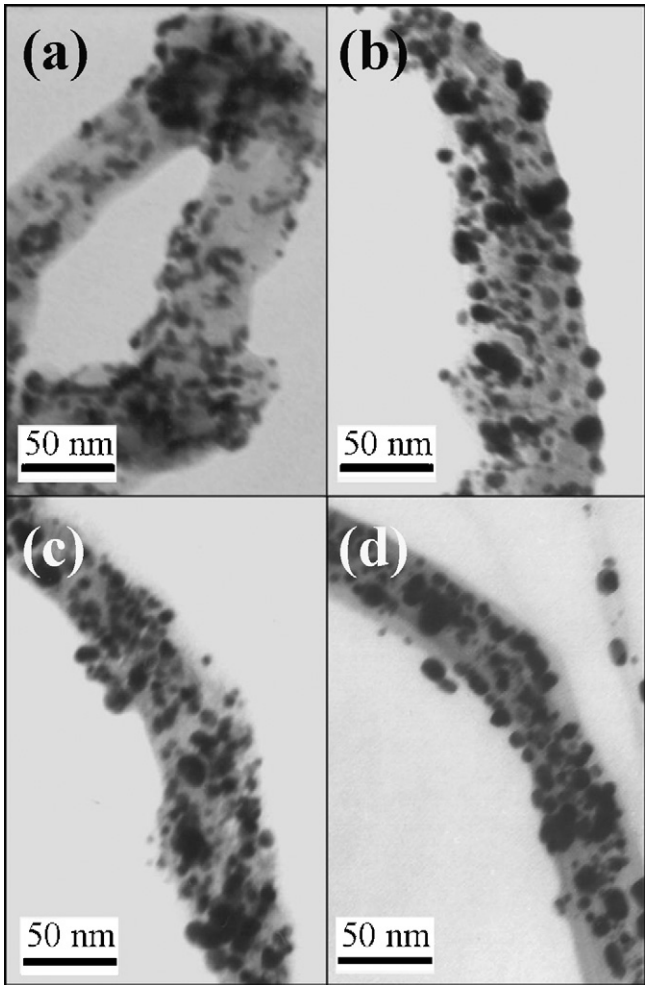

Fig. 3. TEM images of different types of Pt and Pt–M/CNT samples: (a) Pt, (b) Pt–Fe, (c) Pt–Co, and (d) Pt–Ni.

3.2. Methanol oxidation of Pt–M/CNT electrocatalysts

The methanol oxidation investigation for Pt–M/CNT electrocatalysts was evaluated by using CV experiments. Fig. 4(a)–(d) shows cycle voltammograms for CNT electrodes decorated with bimetallic Pt-based catalysts in 1 M H_2SO_4 + 0.5 M CH_3OH at a sweep rate 10 mV s^{-1}. The CV scans start from open-circuit potential and sweep within the entire potential region between 0 V and 1 V vs. SCE. As shown in the CV curves, typical feature of methanol oxidation is observed for all Pt–M/CNT catalysts. However, we observe that the CV profile is significantly affected by the types of bimetallic catalysts. Typically, two oxidation peaks on Pt/CNT catalyst, which are related to the oxidation of methanol and intermediates, appear at 0.67 V and 0.50 V vs. SCE, respectively. With an increase in the cycle number, the oxidation peaks almost maintain the same potentials. The forward scan is attributed to methanol oxidation, forming Pt-adsorbed carbonaceous intermediates, including CO and CO_2. This adsorbed CO causes the loss of activity of the electrocatalyst. The reactions can be expressed as follows [21]:

$$Pt + CH_3OH \rightarrow Pt\text{–}CO_{ads} + 4H^+ + 4e^- \quad (1)$$

$$CH_3OH + H_2O \rightarrow CO_2 + 6H^+ + 6e^- \quad (2)$$

The backward oxidation peak (as shown in reaction (3)) can be attributed to the additional oxidation of the adsorbed carbonaceous species to CO_2:

$$Pt\text{–}CO_{ads} + H_2O \rightarrow Pt + CO_2 + 2H^+ + 2e^- \quad (3)$$

Based on the above deduction, the ratio of the forward peak current (I_f) to the backward peak current (I_b) reflects the ratio of the amount of methanol oxidized to carbon dioxide to the amount of carbon monoxide.

As for Pt–M/CNT catalysts, two oxidation peaks show an obvious shift within 30 cycles. After 30 cycles, the oxidation peaks of different types of Pt–M/CNT catalysts are given as follows: Pt–Fe (0.84 V and 0.70 V vs. Ag/AgCl), Pt–Co (0.68 V and 0.48 V vs. Ag/AgCl), and Pt–Ni (0.75 V and 0.52 V vs. Ag/AgCl). This difference between the oxidation peaks reveals that the performance of methanol oxidation is strongly dominated by different pairs of Pt–M catalysts. The result indicates that the addition of transition metals leads to a higher anodic peak potential, resulting in the delay of methanol oxidation. The phenomena become more evident especially for Pt–Fe catalyst. However, the other catalysts (Pt–Co and Pt–Ni catalysts), just show a little influence in comparison with the pure Pt catalyst.

An observation from Fig. 4(a)–(d) is that the current densities of methanol oxidation are significantly enhanced after the introduction of transition metals, e.g., Pt (300 mA g^{-1}) < Pt–Fe (3150 mA g^{-1}) < Pt–Ni (4050 mA g^{-1}) < Pt–Co (5075 mA g^{-1}) at the 30th cycle. Obviously, Pt–Co/CNT exhibits the best electrocatalysis performance in methanol oxidation. Additionally, it is noted that the onset of methanol oxidation has the following order: Pt/CNT (0.17 V) < Pt–Co/CNT (0.18 V) > Pt–Ni/CNT (0.19 V) > Pt–Fe/CNT (0.21 V), as listed in Table 1. It is generally recognized that the onset potential can be an indicator in determining the electrochemical activity for methanol oxidation [1,6]. This sequence reveals that the first three catalysts, Pt, Pt–Co, and Pt–Ni, show a fairly good electrocatalysis capability in the methanol oxidation.

Another important index, I_f/I_b ratio, in evaluating the activity of methanol oxidation is shown in Table 1. Basically, a higher I_f/I_b value represents a relatively complete oxidation of methanol, producing carbon dioxide [1]. In other words, this ratio essentially reflects the fraction of the catalyst surface that is not poisoned by CO adsorption

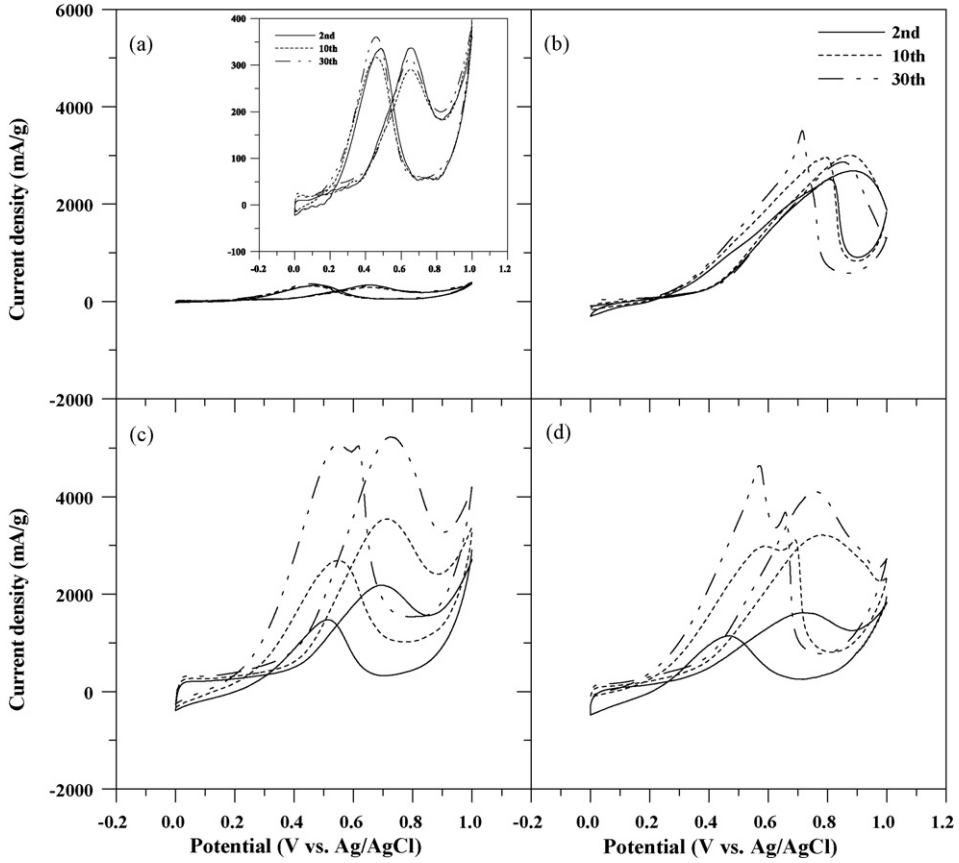

Fig. 4. Cyclic voltammograms of methanol electrooxidation on different types of Pt and Pt–M/CNT electrodes: (a) Pt, (b) Pt–Fe, (c) Pt–Co, and (d) Pt–Ni. Measurements were performed in 1 M H_2SO_4 + 0.5 M CH_3OH with a scan rate of 10 mV s^{-1} and each arrow in the figures indicates an increase of cycle number.

Table 1
Comparison of electrochemical activities of the catalysts.

Catalyst type	Onset potential (V vs. Ag/AgCl)	I_f/I_b at 1st cycle (dimensionless)	I_f/I_b at 30th cycle (dimensionless)
Pt	0.17	1.01	0.87
Pt–Fe	0.21	1.08	0.82
Pt–Co	0.18	1.47	1.03
Pt–Ni	0.19	1.42	0.90

and can be used to measure the catalyst tolerance to CO poisoning [6]. We observe from Table 1 that all bimetallic Pt–M catalysts exhibit high I_f/I_b values by at least 8–40% higher than that in pure Pt catalyst at the first cycle. Such high current ratio represents that most of the intermediate carbonaceous species can be oxidized to carbon dioxide in the forward scan on Pt–M/CNT catalysts [1]. After 30 cycles, Pt–Co/CNT catalyst still has the highest I_f/I_b value of 1.03, which is higher than that in the Pt/CNT catalyst (I_f/I_b ratio: 0.87). The corresponding value of the Pt–Co catalyst is an indication of reduced CO poisoning when compared with that in the pure Pt catalyst.

The current ratio is commonly used to compare long-term catalytic activity between different pairs of Pt–M catalysts. This cycle stability of electrocatalysts for methanol oxidation is the crucial factor in practical application of DMFCs [4]. Fig. 5 shows the long-term cycleability of various catalysts in aqueous electrolyte of 1 M H_2SO_4 + 0.5 M CH_3OH. Among these catalysts, the I_f/I_b ratio of Pt–Co/CNT catalyst maintains the highest value of 1.01 after 100 scans, thus confirming an excellent tolerance to CO. Since the current density of the oxidation peak in anodic scan is almost equal to that in the cathodic scan, this implies that the voltammetric currents mostly arise from the direct oxidation of methanol into CO_2. However, the values of I_f/I_b are only 0.78, 0.80, and 0.89 for Pt/CNT, Pt–Fe/CNT, and Pt–Ni/CNT catalysts, respectively. Based on the above results, including the onset potential of methanol oxidation, forward peak potential, and ratio of the forward anodic peak current to the reverse anodic peak current (I_f/I_b), it can be concluded shown that Pt–Co/CNT catalyst has the greatest catalysis ability in the electrochemically oxidation of methanol.

3.3. Possible mechanism of methanol oxidation on Pt–M/CNT electrocatalysts

On the basis of the above experimental results, Pt–Co/CNT catalyst has better electrochemical activity, antipoisoning ability, and long-term cycleability than in the other three electrocatalysts. This

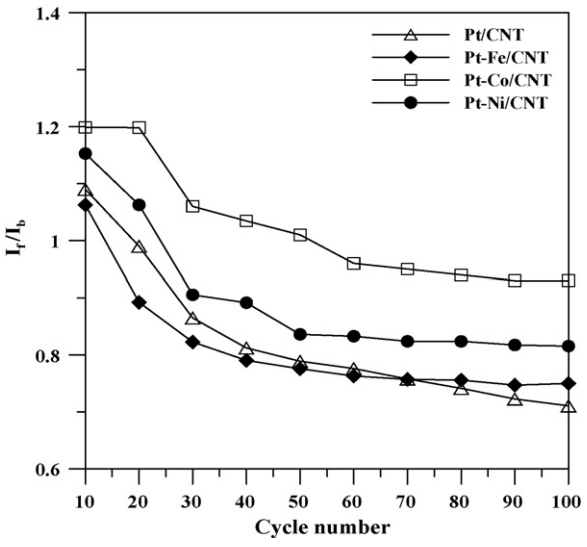

Fig. 5. Variation of I_f/I_b ratio with cycle number for all electrocatalysts.

enhancement of the performance can be explained by two postulations, which should consider adsorption properties of CO and OH surface species. According to the bifunctional theory [31], an efficient catalyst favors CO adsorption on Pt and OH formation takes place on the second metal. For Pt–Ru catalyst, Pt is the most facile for methanol dehydrogenation because of its ability to easily strip hydrogen from the carbon, whereas dehydrogenation of water is more facile on Ru [22]. Hence, the binary combination, atomic ratio of Pt:Ru (1:1), yields the best overall activity for methanol oxidation. Regarding Pt–Co catalyst, two possible pathways for CO adsorption and OH formation can be proposed, according to the bifunctional mechanism. CO adsorption mainly occurs on Pt, while OH species easily interact with Co surface, when compared with Pt–Ru catalyst. Here the secondary metal (i.e., cobalt) is believed to promote electrocatalytic activity and moderate the poisoning of Pt catalyst by supplying OH or other oxygen-containing groups. Since Co skin covers over the Pt core by a two-step chemical reduction process, the OH formation would take place preferentially on the Co surface. Thus, the proximity of CO- and OH-adsorbed species facilitates the enhanced effect of CO oxidation on Pt–Co catalyst, leading to a high-level of CO-tolerance in methanol oxidation. Meanwhile, Pt–Co catalyst appears to offer more active surface sites for methanol oxidation because of the activation of surface coverage of adsorbed species.

The second explanation is another type of the similar bifunctional effect. Before the deposition of the bimetallic catalyst, chemical-wet oxidation in nitric acid generates a large amount of surface oxides on the sidewalls of CNTs. The remaining oxides, such as carboxylic and hydroxyl groups, would aid in the regeneration of Pt–CO_{ads} sites [4], depicted as follows:

$$CNT\text{–}OH + Pt\text{–}CO_{ads} \rightarrow CNT + Pt + CO_2 + H^+ + e^- \quad (4)$$

The above reaction illustrates the other pathway to strip adsorbed CO from the poisoned Pt sites. It is generally known that CNT defects with high reactivity, e.g., dangling bonds, are easier to be oxidized to oxygen-containing groups at low potential. The introduction of transition metals in the bimetallic catalyst reduces the required potential for water electrolysis and thus the associated carbon oxidation [32]. The reaction is tentatively expressed as

$$CNT + Pt\text{–}Co + H_2O \rightarrow CNT\text{–}OH + Pt\text{–}Co\text{–}H \quad (5)$$

The functional surface oxides would be generated continuously on CNT defects during CV scans, thus limiting CO poisoning. The presence of cobalt would promote the combined effect of water dissociation and CO oxidation, creating a larger number of active sites for methanol oxidation. However, an optimal Pt–Co atomic ratio on improvement of catalyst activity and methanol electrooxidation still needs deeper investigation.

To confirm the long-term performance of various Pt–M/CNT catalysts toward methanol oxidation, a chronoamperometry test at a constant potential of 0.45 V vs. Ag/AgCl was conducted for a period of 10 h. Fig. 6 shows the chronoamperometry curves for all catalysts in aqueous electrolyte of 1 M H_2SO_4 + 0.5 M CH_3OH. In the initial stage, all potentiostatic currents are found to decrease rapidly, corresponding to the formation of intermediate species such as CO_{ads}, CH_3OH_{ads}, and CHO_{ads} during methanol oxidation reaction [33]. After a long period of 4 h, the current decay becomes gradual

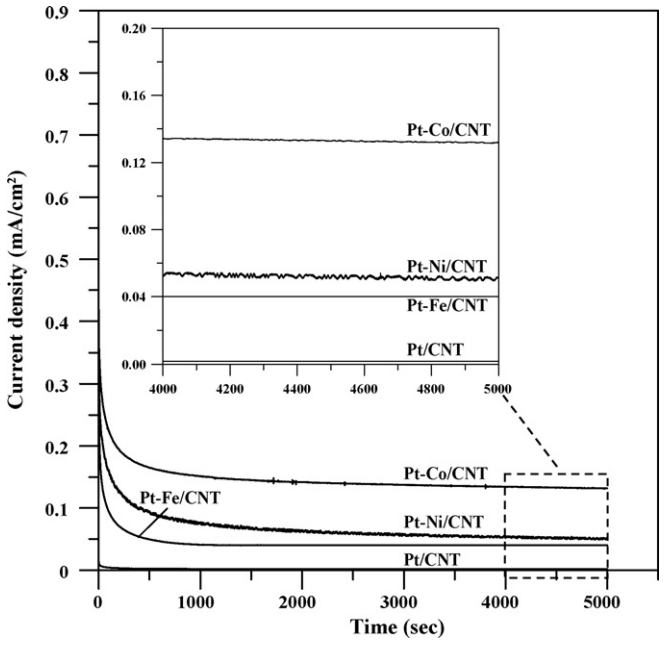

Fig. 6. Current–time curves for methanol oxidation at 0.45 V all electrocatalysts.

and then remains stable. This long time decay is attributed to the fact that surface-adsorbed SO_4^{2-} anions on the bimetallic catalysts would restrict methanol oxidation reaction [34]. The steady-state polarization curves reveal that the stable current of Pt–Co/CNT electrode is higher than in the other three catalysts. This result indicates that Pt–Co catalyst has the highest electrocatalytic activity toward electrooxidation of methanol and stability, which is identical with the results of CV measurements. This proves that bimetallic Pt–Co catalyst seems to be a promising candidate for the DMFCs applications.

4. Conclusions

In this paper we have demonstrated an efficient fabrication of bimetallic Pt–M (M = Fe, Co, and Ni) catalysts in the electrooxidation of methanol, using oxidized CNTs as the catalyst support, and ethylene glycol and hydrogen as the reduction agents. Under our experimental conditions, three catalysts with a similar Pt:M atomic ratio, Pt–Fe (75:25), Pt–Co (75:25), and Pt–Ni (72:28), were prepared for the investigation of methanol oxidation. SEM and TEM analyses showed that highly dispersed bimetallic binary nanoparticles were deposited over the surface of CNTs with no obvious particle agglomeration. The bimetallic particles were found to fall within the region of 5–10 nm. Study of the electrooxidation of methanol on the catalysts showed that all the three pairs of catalysts have higher specific activity than that of pure Pt/CNT catalyst. On the basis of the CV results, Pt–Co/CNT catalyst exhibited the highest electrochemical activity, CO tolerance, and long-term cycleability. This enhancement of the catalytic abilities can be attributed to the bifunctional mechanism of bimetallic catalysts. The chronoamperometry test also showed that Pt–Co/CNT catalyst has the highest current density and excellent stability in the long run among the other three catalysts. The fact that the design of bimetallic Pt–M catalysts in fabricating Pt–M/CNT electrodes enhances the electrochemical activity in methanol oxidation has a positive impact on the development of DMFCs.

Acknowledgements

The authors gratefully acknowledge financial support from the Ministry of Education (MOE) and the National Science Council (NSC) in Taiwan, through Project NSC 96-2221-E-155-055-MY2.

References

[1] Y. Lin, X. Cui, C.H.C.M. Yen, Langmuir 21 (2005) 11474–11479.
[2] S.Y. Huang, S.M. Chang, C.L. Lin, C.H. Chen, C.T. Yeh, J. Phys. Chem. B 110 (2006) 23300–23305.
[3] J. Prabhuram, T.S. Zhao, Z.X. Liang, R. Chen, Electrochim. Acta 52 (2007) 2649–2656.
[4] J. Chen, M. Wang, B. Liu, Z. Fan, K. Cui, Y. Kuang, J. Phys. Chem. B 110 (2006) 1775–1779.
[5] D.A. Stevens, J.R. Dahn, J. Electrochem. Soc. 150 (2003) 770–775.
[6] W. Chen, J. Kim, S. Sue, S. Chen, Langmuir 23 (2007) 11303–11310.
[7] Z. Liu, J.Y. Lee, W. Chen, M. Han, L.M. Gan, Langmuir 20 (2004) 81–87.
[8] L. Li, Y. Xing, J. Phys. Chem. C 111 (2007) 803–808.
[9] L.C. Nagle, J.F. Rohan, J. Power Sources 185 (2008) 411–418.
[10] C.T. Hsieh, Y.W. Chou, W.Y. Chen, J. Alloys Compd. 466 (2008) 233–240.
[11] G. Che, B.B. Lakshmi, C.R. Martin, E.R. Fisher, Langmuir 15 (1999) 750–758.
[12] A. Kongkanand, S. Kuwabata, G. Girishkumar, P. Kamat, Langmuir 22 (2006) 2392–2396.
[13] K.T. Jeng, C.C. Chien, N.Y. Hsu, W.M. Huang, S.D. Chiou, S.H. Lin, J. Power Sources 164 (2007) 33–41.
[14] C.C. Chien, K.T. Jeng, Mater. Chem. Phys. 99 (2006) 80–87.
[15] M.Y. Wang, J.H. Chen, Z. Fan, H. Tang, G.H. Deng, D.L. He, Y.F. Kuang, Carbon 42 (2004) 3257–3260.
[16] D.M. Han, Z.P. Guo, Z.W. Zhao, Y.Z. Meng, D. Shu, H.K. Liu, J. Power Sources 184 (2008) 361–369.
[17] C. Dupont, Y. Jugnet, D. Loffreda, J. Am. Chem. Soc. 128 (2006) 9129–9136.
[18] E.I. Santiago, L.C. Varanda, H.M. Villullas, J. Phys. Chem. C 111 (2007) 3146–3151.
[19] J.R.C. Salgado, E. Antolini, E.R. Gonzalez, J. Phys. Chem. B 108 (2004) 17767–17774.
[20] T. Lopes, E. Antolini, F.R. Gonzalez, J. Power Sources 164 (2007) 111–114.
[21] C.H. Yen, K. Shimizu, Y.Y. Lin, F. Bailey, I.F. Cheng, C.M. Wai, Energy Fuels 21 (2007) 2268–2271.
[22] J. Kua, W.A. Goddard III, J. Am. Chem. Soc. 121 (1999) 10928–10941.
[23] Y. Xu, A.V. Ruban, M. Mavrikakis, J. Am. Chem. Soc. 126 (2004) 4717–4725.
[24] H. Yamada, T. Hirai, I. Moriguchi, T. Kudo, J. Power Sources 164 (2007) 538–543.
[25] C.T. Hsieh, Y.W. Chou, J.Y. Lin, Int. J. Hydrogen Energy 32 (2007) 3457–3464.
[26] K. Kinoshita, Carbon: Electrochemical and Physicochemical Properties, John & Wiley, New York, 1987.
[27] W. Chen, Q. Xin, G. Sun, Q. Wang, Q. Mao, H. Su, J. Power Sources 180 (2008) 199–204.
[28] E.S. Steigerwalt, G.A. Deluga, C.M. Lukehart, J. Phys. Chem. B 106 (2002) 60–66.
[29] Y. Shao, G. Yin, Y. Gao, P. Shi, J. Electrochem. Soc. 153 (2006) A1093–A1097.
[30] S. Kim, S.J. Park, J. Power Sources 159 (2006) 42–45.
[31] M. Watanabe, S. Motoo, J. Electroanal. Chem. 60 (1975) 267–273.
[32] Y. Shao, G. Yin, Y. Gao, P. Shi, J. Electrochem. Soc. 153 (2006) 1093–1097.
[33] A. Kabbabi, R. Faure, R. Durand, B. Beden, F. Hahn, J.M. Leger, C. Lamy, J. Electroanal. Chem. 444 (1998) 41–53.
[34] J. Jiang, A. Kucernak, J. Electroanal. Chem. 543 (2003) 187–199.